International Journal of Heat and Mass Transfer 51 (2008) 5040–5051

Contents lists available at ScienceDirect

International Journal of Heat and Mass Transfer

journal homepage: www.elsevier.com/locate/ijhmt

# Visualization of natural convection heat transport using heatline method in porous non-isothermally heated triangular cavity

Yasin Varol [a,*], Hakan F. Oztop [b], Moghtada Mobedi [c], Ioan Pop [d]

[a] Department of Mechanical Education, Firat University, 23119 Elazig, Turkey
[b] Department of Mechanical Engineering, Firat University, 23119 Elazig, Turkey
[c] Department of Mechanical Engineering, Izmir Institute of Technology, 35430 Izmir, Turkey
[d] Faculty of Mathematics, University of Cluj, CP 253, 3400 Cluj, Romania

ARTICLE INFO

*Article history:*
Received 29 January 2008
Received in revised form 4 April 2008
Available online 6 June 2008

*Keywords:*
Porous medium
Natural convection
Triangular enclosure
Non-isothermal temperature profile
Heatline

ABSTRACT

Natural convection heat transfer in a porous media filled and non-isothermally heated from the bottom wall of triangular enclosure is analyzed using finite difference technique. Darcy law was used to write equations of porous media. Dimensionless heatfunction was used to visualize the heat transport due to buoyancy forces. Three different boundary conditions were applied for the vertical and inclined boundaries of triangular enclosures as Case I; both vertical and inclined walls were isothermal, Case II; vertical wall was adiabatic and inclined one was isothermal, Case III; vertical wall is isothermal and inclined one is adiabatic. A cosine function was utilized to get non-isothermal wall condition. The study was performed for different aspect ratios ($0.25 \leqslant AR \leqslant 1.0$) and Darcy-modified Rayleigh numbers ($100 \leqslant Ra \leqslant 1000$). It was observed that heat transfer enhancement was formed when vertical and inclined walls were isothermal while bottom wall was at non-uniform temperature. Heat transfer from bottom wall did not vary when the value of aspect ratio was higher than 0.50. In addition, heatline visualization technique was a useful technique for non-isothermally heated and porous media filled triangular enclosures.



## 1. Introduction

Analysis of fluid-saturated porous media is an important issue in engineering due to its wide applications in the areas geophysics, heat exchangers, ground-coupled heat pumps, solar collectors, reactors, grain storage, etc. As indicated by wide review studies of Nield and Bejan [1], Vafai [2], Ingham and Pop [3], it is an interdisciplinary topic.

Natural convection phenomena in different shaped enclosures filled with fluid-saturated porous media is also important in engineering applications due to knowledge of flow field and temperature distribution help to design high efficient thermal systems. In the past years, most of the researchers focused on investigation of natural convection in porous square or rectangular enclosures with constant temperature or heat flux boundary conditions as reported in the literature by Bejan [4], Goyeau et al. [5], Gross et al. [6], Manole and Lage [7], Saeid and Pop [8], Baytas and Pop [9]. However, non-isothermal boundary conditions are also faced in practice. The numbers of studies on non-isothermal boundary conditions are limited for enclosures filled with clear fluids [10–12] and cavities filled with fluid-saturated porous media [13,14]. The shape of enclosure can be different than rectangular geometry such as triangle [15,16], parallelogram [17] or trapezoidal enclosures [18–21] depending on application requirements. To our best knowledge, the problem of natural convection in a triangular enclosure filled with fluid-saturated porous media with non-isothermal boundary conditions has not been investigated before.

Heatline technique is an important method to visualize heat transport in enclosures filled clear fluids or fluid-saturated porous media. Isotherms are used to show the temperature distribution in a domain, however, it is not easy to realize the direction and intensity of heat transfer particularly in convection problems in which path of heat flux is not perpendicular to isotherm due to convection effect. Heatline is a useful tool for visualization and analysis of not only direction but also intensity of heat transfer in a domain. They provide corridors in where heat is transferred from hot to the cold regions by convection and/or conduction. Heatline technique was first proposed by Kimura and Bejan [22] to visualize the convective heat transfer and the method has been extended to different applications by Morega and Bejan [23], Dash [24], Dalal and Das [25] and Costa [26]. A detailed review study on applications of heatlines was performed by Costa [27]. The method has been also applied to conjugate heat transfer by Zhao et al. [28], Mobedi [29], Deng and Tang [30]. They indicated that the heatline visualization is a powerful method to show the heat interaction between solid and fluid at an interface.

* Corresponding author. Tel.: +90 424 237 0000x4219; fax: +90 424 236 7064.
*E-mail address:* ysnvarol@gmail.com (Y. Varol).

0017-9310/$ - see front matter © 2008 Elsevier Ltd. All rights reserved.
doi:10.1016/j.ijheatmasstransfer.2008.04.023

**Nomenclature**

| | |
|---|---|
| AR | aspect ratio parameter, ($H/L$) |
| $g$ | gravitational acceleration (m s$^{-2}$) |
| $h$ | dimensional heatfunction |
| $H$ | height of triangle, dimensionless heatfunction, $H = h/(T_H - T_C)k$ |
| $K$ | permeability of the porous medium (m$^2$) |
| $L$ | length of the bottom wall (m) |
| $Nu_x$ | local Nusselt number, $Nu_x = (-\partial\theta/\partial Y)_{Y=0}$ |
| $Ra$ | Darcy-modified Rayleigh number, $Ra = (g\beta K(T_H - T_C)L)/\upsilon\alpha_a$ |
| $T$ | fluid temperature (K) |
| $u,v$ | velocity components along $x$- and $y$-axes, respectively (m s$^{-1}$) |
| $U,V$ | non-dimensional velocity components along $x$- and $y$-axes, respectively, ($uL/\alpha_a, vL/\alpha_a$) |
| $x,y$ | dimensional Cartesian coordinates (m) |
| $X,Y$ | non-dimensional coordinates, ($X = x/L, Y = y/L$) |

*Greek symbols*

| | |
|---|---|
| $\alpha_a$ | thermal diffusivity of porous media (m$^2$ s$^{-1}$) |
| $\beta$ | thermal expansion coefficient (K$^{-1}$) |
| $\lambda$ | amplitude of the sinusoidal temperature distribution |
| $\theta$ | non-dimensional temperature, $\theta = (T - T_C)/(T_H - T_C)$ |
| $\upsilon$ | kinematic viscosity (m$^2$ s$^{-1}$) |
| $\psi$ | dimensional stream function (m$^2$ s$^{-1}$) |
| $\Psi$ | non-dimensional stream function, $\Psi = \psi/\alpha_a$ |

*Subscripts*

| | |
|---|---|
| $C$ | cold |
| $H$ | hot |
| max | maximum |

The main purpose of this study is to visualize heat transport due to natural convection in a non-isothermally heated triangular enclosure filled with a fluid-saturated porous medium based on Darcy equation model. The above literature review clearly shows that the earlier studies did not investigate the visualization of heat transport in porous triangular enclosures. Thus, the present work is the first attempt at studying on that research area under the above mentioned thermal conditions and geometry. However, the problem can be easily extended to the case when the inertia effects have to be incorporated (Al-Amiri [31]).

## 2. Definition of physical model

Considered the physical model of a right-angle triangular enclosure filled with a fluid-saturated porous medium with length of bottom wall, $L$, and height of vertical wall, $H$, as is illustrated in Fig. 1a. Based on thermal boundary conditions, three different cases were analyzed. For all cases considered the bottom wall is non-isothermal; however the boundary conditions of vertical and inclined walls vary with the case. In Case I, both vertical and inclined walls are isothermal and their temperature is taken as zero. In Case II, the inclined wall is isothermal with $T = T_C$ and vertical wall is adiabatic. The vertical wall of Case III is isothermal ($T = T_C$) and the inclined wall is adiabatic. The gravity acts in the vertical direction. An aspect ratio is defined as AR = $H/L$. Regular grid was used for all cases as given in Fig. 1b.

## 3. Governing equations

The dimensional set of the governing equations of the present problem are the continuity, Darcy law and energy given by Eqs. (1)–(3). Properties of the fluid and the porous medium are constant; the cavity walls are impermeable; the Boussinesq approximation is valid; and the viscous drag and inertia terms in the momentum (Darcy) equation are neglected (see Nield and Bejan [1]). Under these assumptions, the governing equations can be written as follows:

$$\frac{\partial u}{\partial x} + \frac{\partial v}{\partial y} = 0 \tag{1}$$

$$\frac{\partial u}{\partial y} - \frac{\partial v}{\partial x} = -\frac{g\beta K}{\upsilon}\frac{\partial T}{\partial x} \tag{2}$$

$$u\frac{\partial T}{\partial x} + v\frac{\partial T}{\partial y} = \alpha_a\left(\frac{\partial^2 T}{\partial x^2} + \frac{\partial^2 T}{\partial y^2}\right) \tag{3}$$

where $u$, $v$ are the velocity components along $x$- and $y$-axes, respectively, $T$ is the fluid temperature, $K$ is the permeability of the porous medium and the physical meaning of the other quantities is given in the Nomenclature. The above equations can be written in terms of the stream function $\psi$ defined as

$$u = \frac{\partial \psi}{\partial y}, \quad v = -\frac{\partial \psi}{\partial x} \tag{4}$$

and non-dimensional variables

$$X = \frac{x}{L}, \quad Y = \frac{y}{L}, \quad \theta = \frac{T - T_C}{T_H - T_C}, \quad \Psi = \frac{\psi}{\alpha_a}, \quad U = \frac{uL}{\alpha_a}, \quad V = \frac{vL}{\alpha_a} \tag{5}$$

where $Ra$ is the Darcy-modified Rayleigh number defined as

$$Ra = \frac{g\beta K(T_H - T_C)L}{\upsilon\alpha_a} \tag{6}$$

Thus, Eqs. (1)–(3) can be written in non-dimensional form as

$$\frac{\partial^2 \Psi}{\partial X^2} + \frac{\partial^2 \Psi}{\partial Y^2} = -Ra\frac{\partial \theta}{\partial X} \tag{7}$$

$$\frac{\partial \Psi}{\partial Y}\frac{\partial \theta}{\partial X} - \frac{\partial \Psi}{\partial X}\frac{\partial \theta}{\partial Y} = \frac{\partial^2 \theta}{\partial X^2} + \frac{\partial^2 \theta}{\partial Y^2} \tag{8}$$

The boundary conditions for the considered model are shown in Fig. 1a. We have also classified them according to three different cases given in Table 1. The non-dimensional sinusoidal temperature distribution on the bottom wall is $\theta = \lambda(1 - \cos(2\pi X))$ and it is $\theta = 2\lambda$ for $X = 0.5$ and we take $\lambda = 0.5$.

Heat function for a dimensional convection problem can be defined as

$$-\frac{\partial h}{\partial x} = \rho c_p v(T - T_C) - k\frac{\partial T}{\partial y} \tag{9}$$

$$\frac{\partial h}{\partial y} = \rho c_P u(T - T_C) - k\frac{\partial T}{\partial x} \tag{10}$$

where $h$ is the dimensional heatfunction. By employing the non-dimensional parameters defined by relations (5), Eqs. (9) and (10) can then be written in dimensionless form Table 2

$$-\frac{\partial H}{\partial X} = V\theta - \frac{\partial \theta}{\partial Y} \tag{11}$$

$$\frac{\partial H}{\partial Y} = U\theta - \frac{\partial \theta}{\partial X} \tag{12}$$

where $H$ is the non-dimensional heat function for the fluid and it is defined as

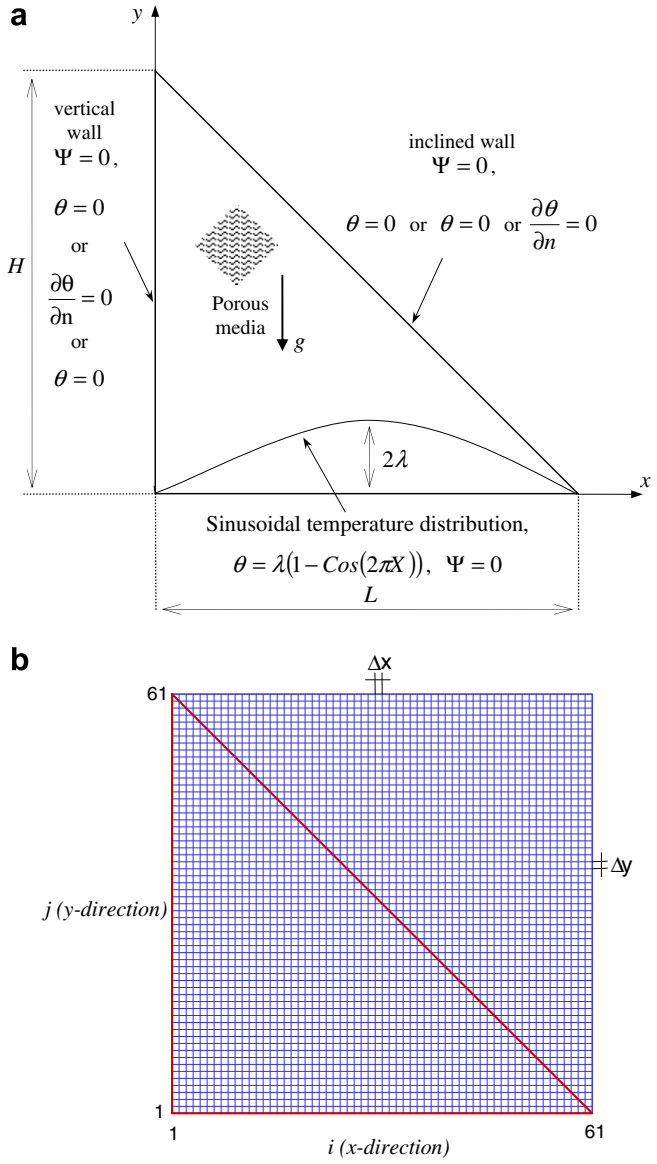


**Fig. 1.** (a) Physical model, (b) finite-difference grid for a triangular enclosure.

**Table 1**
Definitions of boundary conditions

| Wall | Case I | Case II | Case III |
|---|---|---|---|
| Inclined | $\theta = 0$ | $\theta = 0$ | $\frac{\partial\theta}{\partial n} = 0$ |
| Vertical | $0 < Y < H/L, \theta = 0$ | $0 < Y < H/L, \frac{\partial\theta}{\partial X} = 0$ | $0 < Y < H/L, \theta = 0$ |
| Bottom | $0 \leqslant X \leqslant 1, \theta = \lambda(1 - \cos(2\pi X))$ | $0 \leqslant X \leqslant 1,$ $\theta = \lambda(1 - \cos(2\pi X))$ | $0 \leqslant X \leqslant 1, \theta = \lambda$ $(1 - \cos(2\pi X))$ |

$$H = \frac{h}{(T_H - T_C)k} \tag{13}$$

Assuming that $H$ is a continuous function to its second order derivatives it yields the following differential equation for heat function

$$\frac{\partial^2 H}{\partial X^2} + \frac{\partial^2 H}{\partial Y^2} = \frac{\partial(U\theta)}{\partial Y} - \frac{\partial(V\theta)}{\partial X} \tag{14}$$

This equation is a Poisson equation which can be solved numerically. The convection terms which are written on the right side of Eq. (14) act as a source term. The solution of this equation yields

**Table 2**
Grid independency test at AR = 1.0, $Ra$ = 1000 and Case I

| Grid dimension ($X$ by $Y$) | Mean Nusselt number ($Nu$) |
|---|---|
| 31 × 31 | 7.65 |
| 41 × 41 | 8.44 |
| 61 × 61 | 9.37 |
| 81 × 81 | 9.86 |
| 101 × 101 | 9.92 |

**Table 3**
Comparison of mean Nusselt number with the literature at $Ra$ = 1000

| References | $Nu$ |
|---|---|
| Bejan [4] | 15.800 |
| Goyeau et al. [5] | 13.470 |
| Gross et al. [6] | 13.448 |
| Manole and Lage [7] | 13.637 |
| Saeid and Pop [8] | 13.726 |
| Baytas and Pop [9] | 14.060 |
| This study | 13.564 |

**Table 4**
Results for $Ra$ = 100 to compare present results with literature

| Inclined angle | 15° | 30° | 45° |
|---|---|---|---|
| Nu (Ref. [17]) | 2.95 | 2.62 | 2.23 |
| Nu (present) | 2.872 | 2.585 | 2.217 |

dimensionless heatfunction in the inner region of the triangular enclosure considered. The drawing of isolines of the heat function provides heatlines.

The boundary conditions of the non-dimensional heatfunction equation (Eq. 14) are obtained from the integration of differential definition of $H$ along the considered boundary conditions. For example, the heatfunction boundary conditions for Case I triangle are determined as follows:

$$\text{for bottom wall} \quad 0 < X \leqslant 1: \quad H(X,0) = H(0,0) + \int_0^X \frac{\partial\theta}{\partial Y} dX \tag{15}$$

$$\text{for vertical wall} \quad 0 < Y \leqslant H/L: \quad H(0,Y) = H(0,0) - \int_0^Y \frac{\partial\theta}{\partial X} dY \tag{16}$$

$$\text{for inclined wall} \quad 0 < X < 1 \quad \text{and} \tag{17}$$

$$0 < Y \leqslant H/L: \quad H(X,Y) = H(1,0) - \int_{\ell=0}^{\ell} \frac{\partial\theta}{\partial n} d\ell \tag{18}$$

where $d\ell$ is the differential distance on the inclined wall and $n$ shows the normal direction of the inclined wall that points outward. The value of heatfunction at the origin is $H(0,0) = 0$.

The physical quantities of interest in this problem are the local and mean Nusselt numbers, which for bottom wall are given by

$$Nu_x = \left(-\frac{\partial\theta}{\partial Y}\right)_{Y=0}, \quad Nu = \int_0^1 Nu_x dX \tag{19}$$

## 4. Numerical implementation

Finite difference method is used to solve the governing equations, Eqs. (7), (8) and the heatfunction equation, (14). Central difference method is applied for discretization of these equations. The

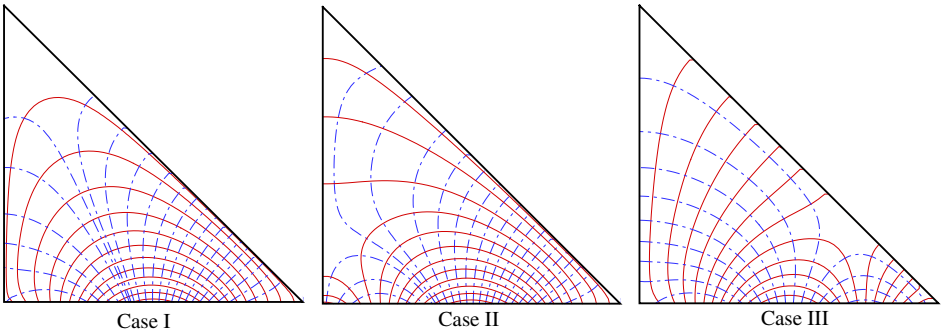


**Fig. 2.** Isotherms and heatlines in the cavity for different cases at $Ra = 0$ and $AR = 1.0$ (red lines: isotherms, blue dash lines: heatline). (For interpretation of the references to colour in this figure legend, the reader is referred to the web version of this article.)

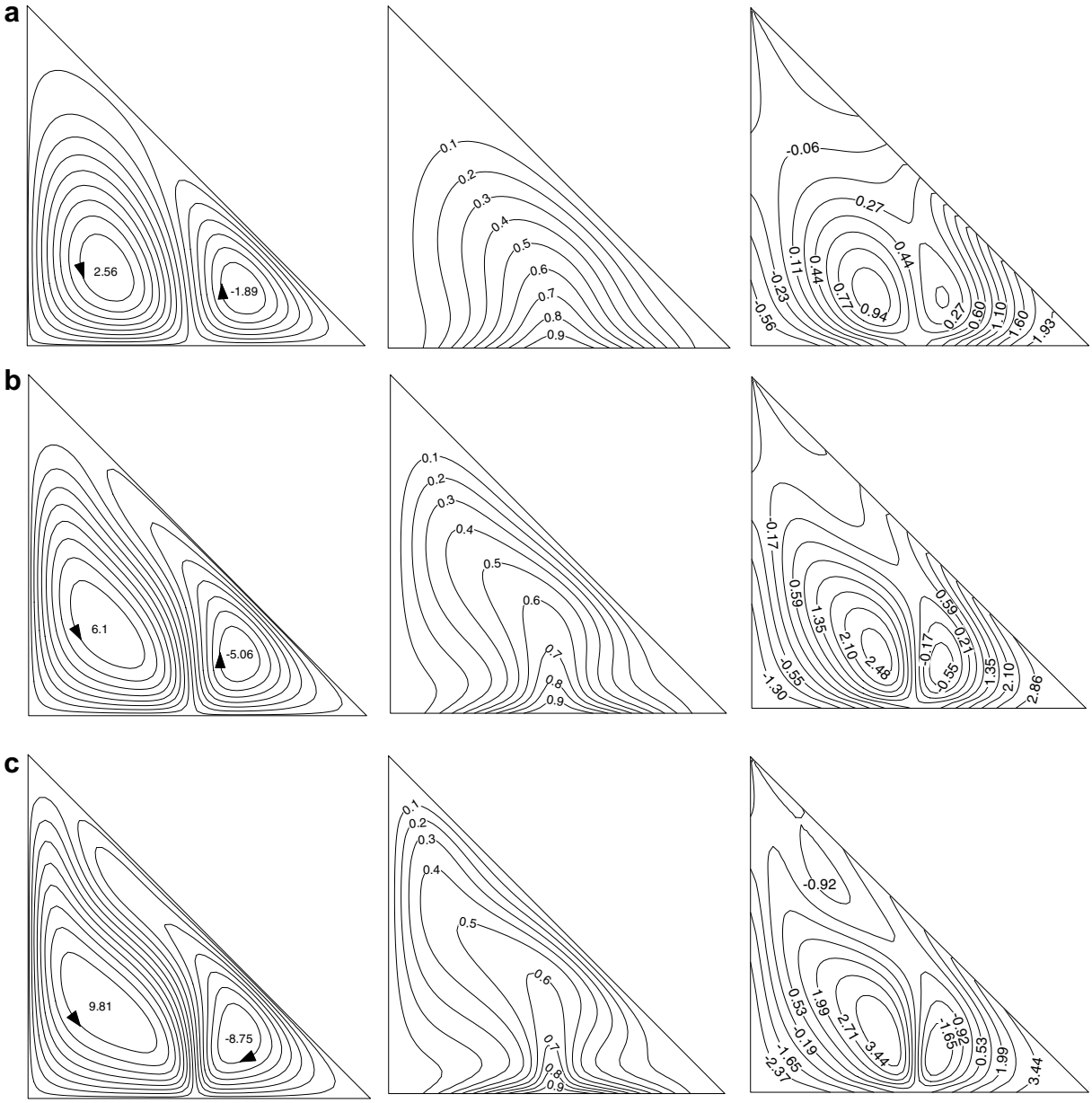


**Fig. 3.** Streamlines (left), isotherms (middle) and heatlines (right) in the cavity for different Darcy-modified Rayleigh numbers at $AR = 1.0$ and Case I, (a) $Ra = 100$, (b) $Ra = 250$, (c) $Ra = 500$.

solution of linear algebraic equations was performed using successive under relaxation (SUR) method. The following convergence criterion is employed for termination of procedure

$$\frac{|\theta^{P+1} - \theta^{P}|}{\theta^{P}} \leqslant 10^{-4} \tag{20}$$

The same criterion was used to obtain the solution of heatfunction equation, Eq. (14). For the solution of all depended variables in Eqs. (7), (8) and (14) the value of 0.1 is taken for under-relaxation parameter. The uppermost grid-point on each vertical grid line coincided with the top wall of the triangular enclosure as indicated by Haese and Teubner [32] and Asan and Namli [15], as seen in Fig. 1b. The inclined wall was approximated with staircase-like zigzag lines. Table 1 shows a serial tests on grid-independency against the mean Nusselt number for the Case I and AR = 1.0 and *Ra* = 1000. As seen from this table, grid sizes from 31 × 31 to 101 × 101 were tried. The number of grid points is taken as 61 × 61 with uniform spaced mesh in both *X*- and *Y*-directions. It should be mentioned that the numerical algorithm used in this study was tested with the problem of classical natural convection heat transfer in a differentially heated square porous enclosure. Published experimental data are not available for the cavity configuration and boundary conditions considered in this study. Thus, the validation of achieved results against suitable experimental data could not be performed. However, the numerical results were also obtained for a square cavity configuration and compared with the results reported by different authors as tabulated in Table 3. We used again 61 × 61 grid points for this test. As can be seen from the table, the obtained results show good agreement with the results from the open literature. Another test was performed for an inclined geometry of Baytas and Pop [17] as listed in Table 4. The present code also gives good results with those of Baytas and Pop [17]. The contours of streamline and isotherms are almost the same to those reported in the literature for rectangular enclosure; however, they are not presented here to save space. For validation of heatfunction results the code was tested by obtaining results for conduction mode of heat transfer, namely, *Ra* = 0. It is well known that the heatline must be normal to the isotherms for pure conduction. As shown in Fig. 2a–c, which represents all cases considered, heatlines and isotherms are perpendicular to each other. Heatfunction equation was also solved for square cavity with differential wall temperatures and compared with the results of Deng and Tang [30]. Obtained results from the present code showed good agreement with this study.

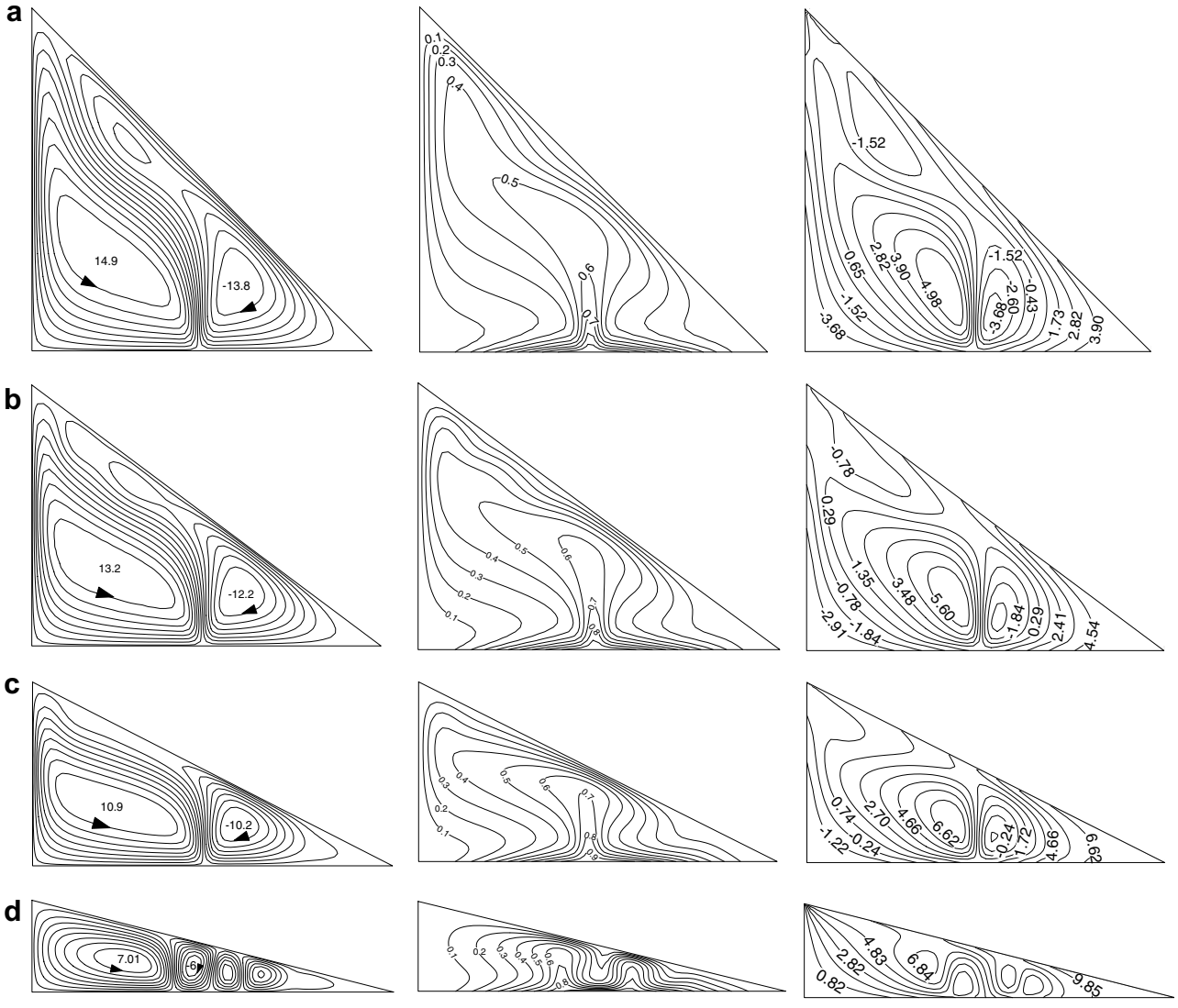


**Fig. 4.** Streamlines (left), isotherms (middle) and heatlines (right) in the cavity for different aspect ratios at *Ra* = 1000 and Case I, (a) *AR* = 1.0, (b) *AR* = 0.75, (c) *AR* = 0.50, (d) *AR* = 0.25.

## 5. Results and discussion

The results of flow fields, temperature distributions, heat transfer and visualization of heat transport with heatline for the porous non-isothermally heated triangular enclosure are examined in this section. The thermal behaviors of the different cases are discussed separately. As it was mentioned before, the bottom wall of the triangular enclosure is heated non-isothermally for the all considered cases.

(a) Case I:Fig. 3 shows the streamline (on the left), isotherms (on the middle) and heatlines (on the right) in a porous triangular enclosure with AR = 1.0 for different values of the Darcy-modified Rayleigh number. We can see that, double circulation cells were formed in different rotating directions, starting from the middle of the bottom wall for all Darcy-modified Rayleigh numbers considered. The cell in left side becomes dominant on right one with increasing of the Darcy-modified Rayleigh number. In other words, the cell formed at the right corner is squeezed to a rather small fraction of the domain. It impinges to the inclined wall and its strength increases with the domination of convection mode of heat transfer. It rotates in clockwise direction but the big cell rotates counterclockwise. The figure also shows the maximum and minimum streamfunction values. As given in the figure, the absolute values of minimum and maximum of streamfunction increase with increasing of the Darcy-modified Rayleigh number which indicates the increase of the flow strength. We can also see from the isotherms that they are distributed almost parallel to each other but plumelike distribution is observed with the increasing of Darcy-modified Rayleigh number. Because of the presence of inclined wall, the isotherms are observed to have skew-

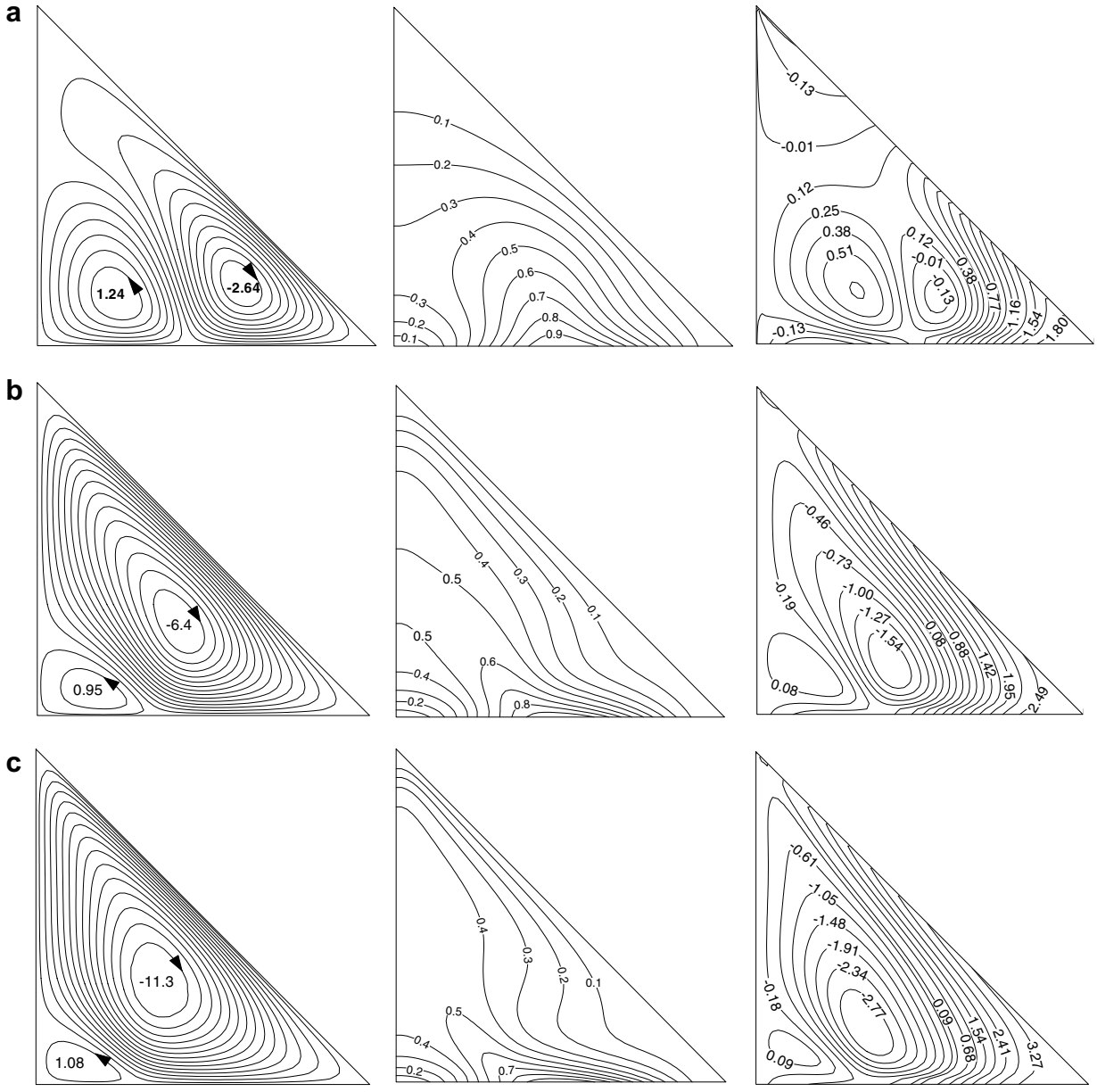


**Fig. 5.** Streamlines (left), isotherms (middle) and heatlines (right) in the cavity for different Darcy-modified Rayleigh numbers at *AR* = 1.0 and Case II, (a) *Ra* = 100, (b) *Ra* = 250, (c) *Ra* = 500.

ness towards to the left vertical wall of the enclosure. The magnitude of heatfunction increases with increasing of Darcy-modified Rayleigh number as is seen from heatline contours. This shows the increase of heat transfer rate from the bottom wall with increase of Darcy-modified Rayleigh number. Two vortices are seen from the heatlines above the heater. The corridors occur between two heatlines shows the path of heat from hot to cold region. As is seen from heatlines of Case I (Fig. 3), heat from the bottom wall is transferred to both vertical and inclined walls.Further, we tested the effects of aspect ratio AR on streamlines, isotherms and heatlines for $Ra = 1000$, which is the highest Darcy-modified Rayleigh number in this study, and results are illustrated in Fig. 4. The value of AR varies in the range of 0.25 and 1.0. For the case of AR = 1.0, a third cell was formed near the top of the triangle. In the similar manner, closed vortices are also observed at heatline. A strong plumelike distribution is also shown from the isotherms due to higher Darcy-modified Rayleigh number. The third cell becomes very small and it disappeared with the decreasing of aspect ratio. Values of streamfunction showed that flow strength decreases with decreasing of aspect ratio. Bénard cells were formed at AR = 0.25 due to small height of the enclosure. In this case, isotherms show wavy variation and four vortices are observed from the heatfunction contours.

(b) Case II:Fig. 5 shows the streamlines (on the left), isotherms (on the middle) and heatfunction contours (on the right) for Case II. The temperature of inclined wall is taken as zero and vertical wall is adiabatic in this case. As given in Case I, two cells were formed inside the enclosure in different rotation direction. On the contrary to the Case I, the right cell becomes dominant to the left one. The left vortices are squeezed to the left bottom corner and its dimension is decreased with increasing of Darcy-modified Rayleigh number. At $Ra = 100$, the circulation inside the enclosure is so weak that the viscous forces are dominant over the buoyancy force. With the increasing of Darcy-modified Rayleigh number, the intensity of the recirculation inside the enclosure increases and hydrodynamic and thermal boundary layers near the walls become thinner. As a result of this, the strength of the fluid increases with increasing of Darcy-modified Rayleigh number. As illustrated in isotherms that for $Ra = 500$, the temperature gradients are confined to

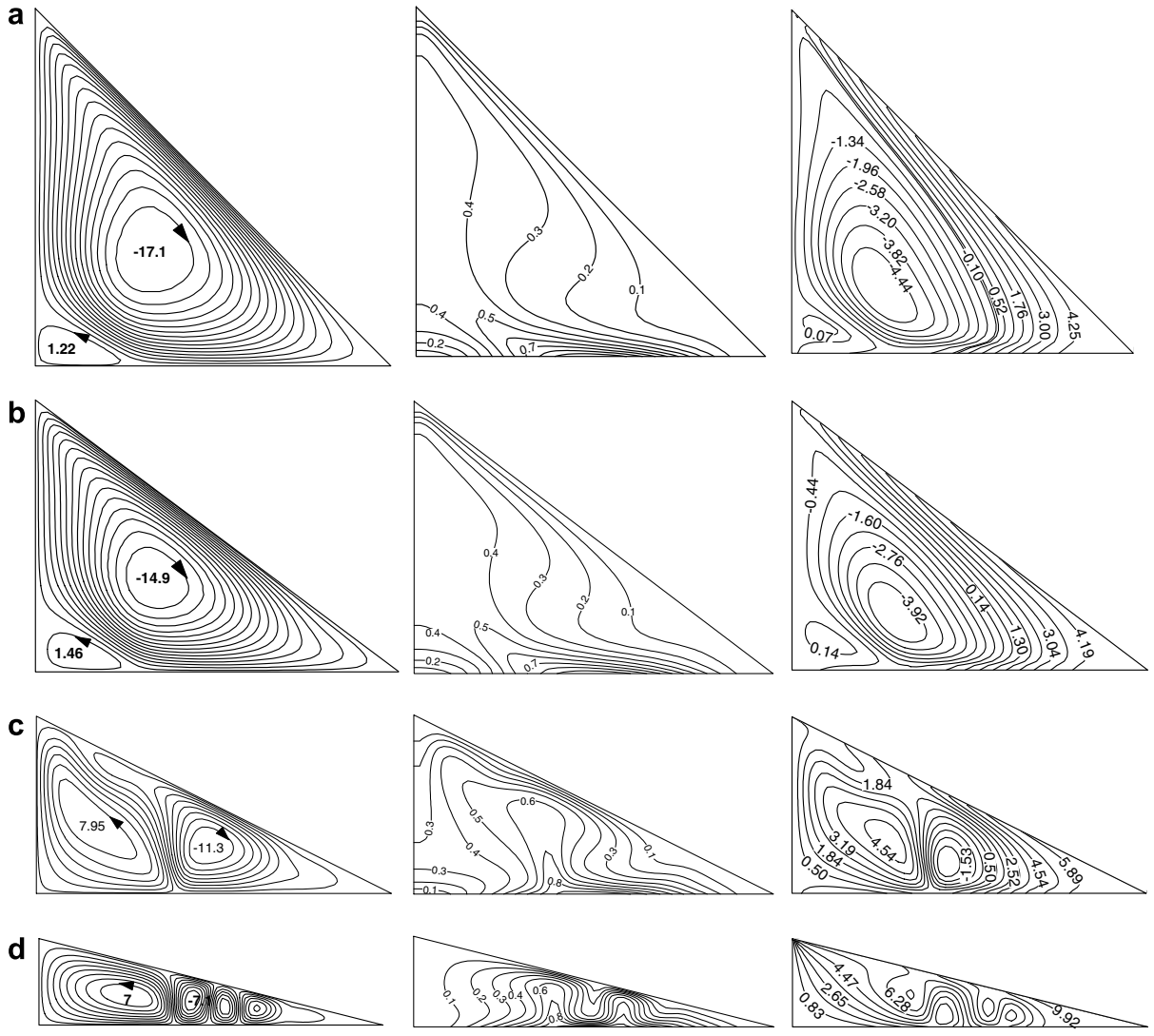


**Fig. 6.** Streamlines (left), isotherms (middle) and heatlines (right) in the cavity for different aspect ratios at $Ra = 1000$ and Case II, (a) $AR = 1.0$, (b) $AR = 0.75$, (c) $AR = 0.50$, (d) $AR = 0.25$.

the bottom wall in the form of a thermal boundary layer. This layer becomes thinner with increasing of Darcy-modified Rayleigh number. Heatfunction contours showed that center of the vortices in heatlines and isotherms are almost in same location since confinement of the flow causes the heat transfer enhancement. This is clear from results for the highest Darcy-modified Rayleigh number which is plotted in Fig. 6. This figure also shows the effects of the aspect ratio AR on flow and temperature field for Case II. Aspect ratio is not significant for AR = 1.0 and AR = 0.75. But in the case of AR = 0.50, the results of streamlines, isotherms and heatlines are similar to the Case I since the height of adiabatic wall (vertical wall) becomes smaller with decreasing of AR. The vertical wall of triangle enclosure is adiabatic and no heat transfers from the bottom or the inclined wall to the vertical wall as seen from heatlines of Case II (Figs. 5 and 6). If the heat transfer corridors for Case II are followed, it will be observed that most of heat in the enclosure is transferred from the hot part of the bottom wall to the inclined wall and in addition heat transfer from hot to cold part of bottom wall arises.

(c) Case III:Boundary conditions are taken in Case III as inclined wall is adiabatic, vertical wall is isothermal ($\theta = 0$) and again bottom wall is non-isothermal. Fig. 7 shows the streamlines (on the left), isotherms (on the middle) and heatlines (on the right) for different Darcy-modified Rayleigh numbers for Case III. As seen from the streamlines plot that two circulation cells were formed as obtained other cases. In this case, left cell is dominant to right one on the contrary of other cases. The cell, which rotates in clockwise rotating direction, is squeezed to the right bottom corner with −0.62. Isotherms plot shows that skewness of the isotherms toward to the inclined wall on the contrary of other cases. Heatlines reveal that the heat

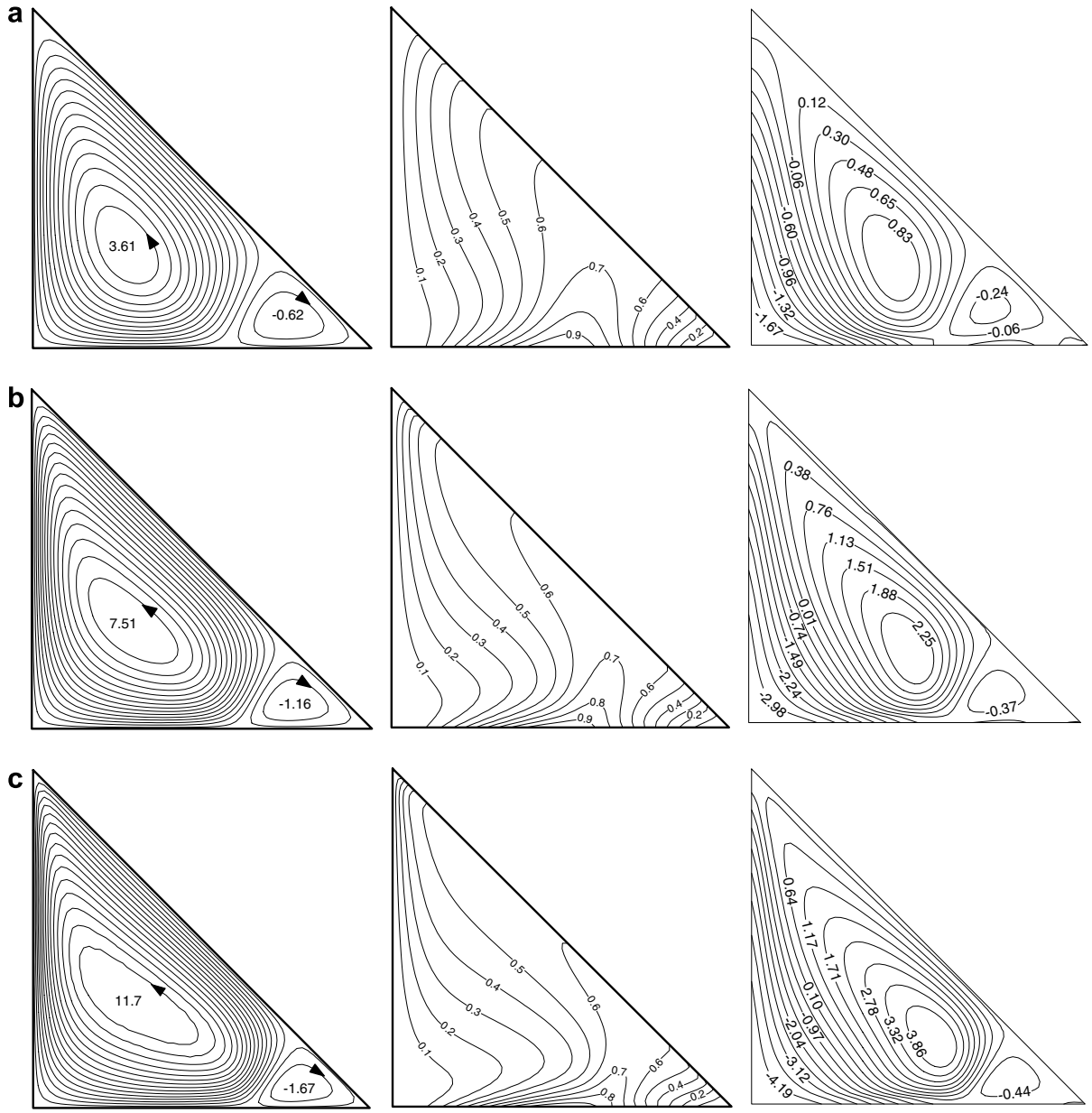


**Fig. 7.** Streamlines (left), isotherms (middle) and heatlines (right) in the cavity for different Darcy-modified Rayleigh numbers at $AR = 1.0$ and Case III, (a) $Ra = 100$, (b) $Ra = 250$, (c) $Ra = 500$.

is transferred from the middle of the non-isothermal source to a large portion of the enclosure. It makes a huge vortex inside the enclosure. Domination of vortices increases with increasing of Darcy-modified Rayleigh number. Again aspect ratio AR is an effective parameter for this case too (Fig. 8). But there is no Bénard cells in this case depend of the boundary conditions. Flow strength decreases with decreasing of aspect ratio. The heatlines of the Case III shows that there is not heat transfer to the inclined wall which is adiabatic. A weak heat transfer from bottom to bottom in the right corner region of enclosure forms, though most of heat in the enclosure is transferred from the bottom to the vertical wall.Variation of the local Nusselt number along the bottom wall is presented in Fig. 9 for different three cases at different Darcy-modified Rayleigh numbers and AR = 1.0. As seen from Fig. 9a that variation of local Nusselt number is symmetrical due to symmetry in the temperature field. As indicated earlier those both vertical and inclined walls have colder than that of bottom wall. Values of local Nusselt number increase with increasing of Darcy-modified Rayleigh number especially at the middle section of the non-isothermal wall due to adding of large amount of heat from that section to the system. As given by the study of Sarris et al. [10], which is performed for viscous fluid filled square enclosure with non-isothermal heating from the ceiling, local Nusselt number is positive at these region. However, local Nusselt numbers are negative at the corners of the bottom wall due to losing of heat (Fig. 9b). In the Case II, again local Nusselt numbers are positive almost right half part of the bottom wall due to increasing of recirculation intensity at that part of the cavity as given from the streamline plots in Figs. 5 and 6. Absolute value of local Nusselt number increases with increasing of Darcy-modified Rayleigh number near the left bottom corner of the triangular enclosure. On the contrary of Case II, positive values are observed at the left part of the bottom wall in Case III depends of the recirculation intensity which is given in Figs. 7 and 8. Local Nusselt number shows sinusoidal wave like variation at the right bottom corner of the enclosure (Fig. 9c). Fig. 10 shows the effects of aspect ratio on variation of local Nusselt number for three cases and $Ra = 1000$. As seen from the figure that local Nusselt numbers show almost symmetrical distribution according to mid-section of the bottom wall for all values of aspect ratio (Fig. 10a). All values are almost positive due to heat

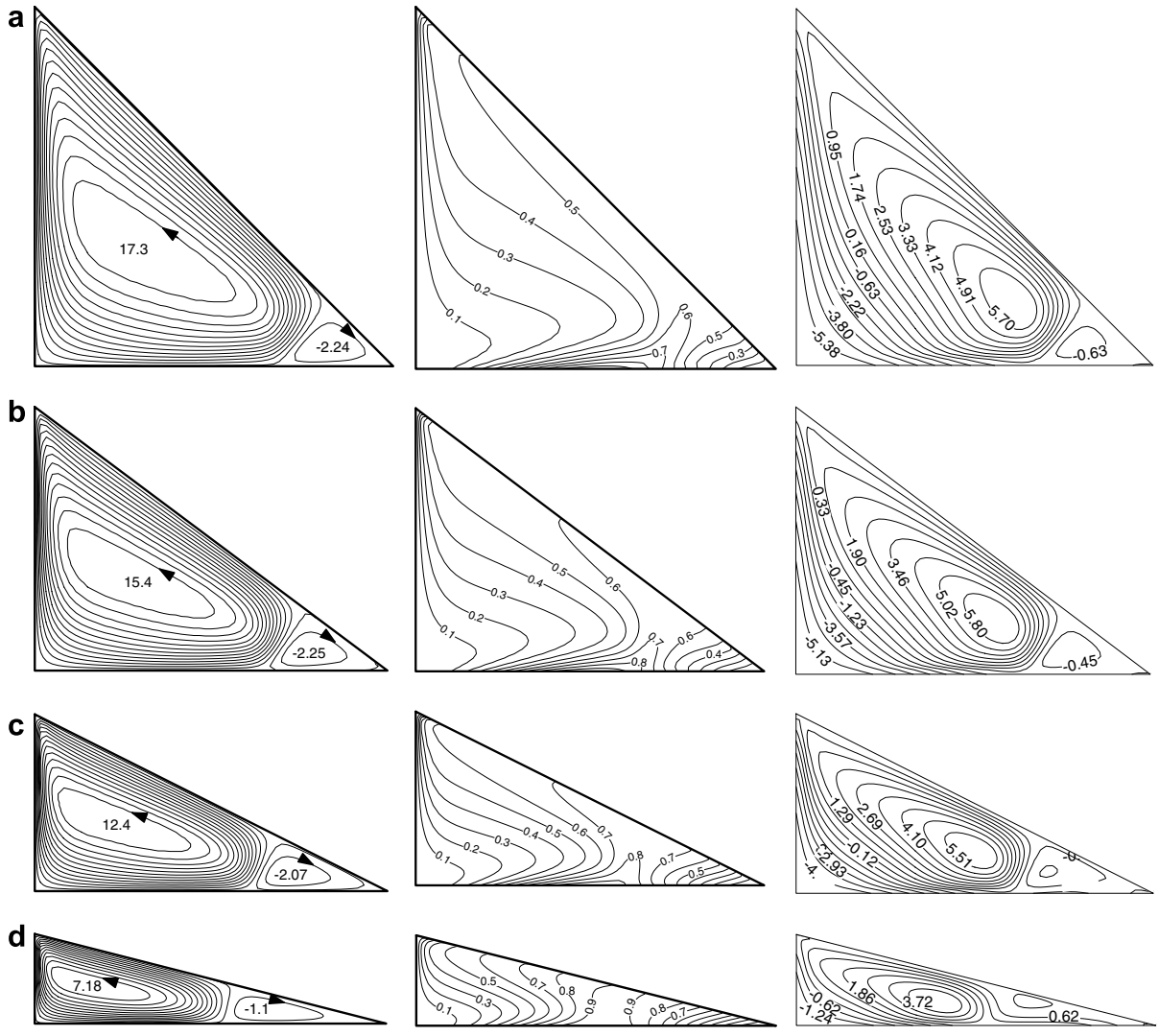


**Fig. 8.** Streamlines (left), isotherms (middle) and heatlines (right) in the cavity for different aspect ratios at $Ra = 1000$ and Case III, (a) $AR = 1.0$, (b) $AR = 0.75$, (c) $AR = 0.50$, (d) $AR = 0.25$.

gain from the non-isothermal heater. A sinusoidal variation has been observed at AR = 0.25 due to forming of Bénard cell at this value of aspect ratio as seen from the Fig. 4d. In the Case II, variation of local Nusselt number for AR = 0.25 is almost the same with Case I. But there is no symmetrical trend for other values of aspect ratio (Fig. 10b). It means that boundary conditions play an extremely important role on heat transfer. In these case, there are negative values near the corners of the bottom wall for AR = 0.50, 0.75 and 1.0. There are two peaks for except AR = 0.25 due to presence of two circulation cells inside the cavity AR. Fig. 10c indicates that heat transfer is positive almost at left half of the bottom wall and negative at the other side. They also indicate that there is no Bénard flow structure inside the cavity even at same parameter with other cases. It means that type of boundary conditions is highly effective on formation of Bénard cells.

### 5.1. Overall heat transfer

We summarized the study by showing the variation of the average Nusselt numbers for three cases at different Darcy-modified Rayleigh numbers. Negative values for the local Nusselt numbers are seen in Fig. 9 due to non-uniform temperature boundary con-

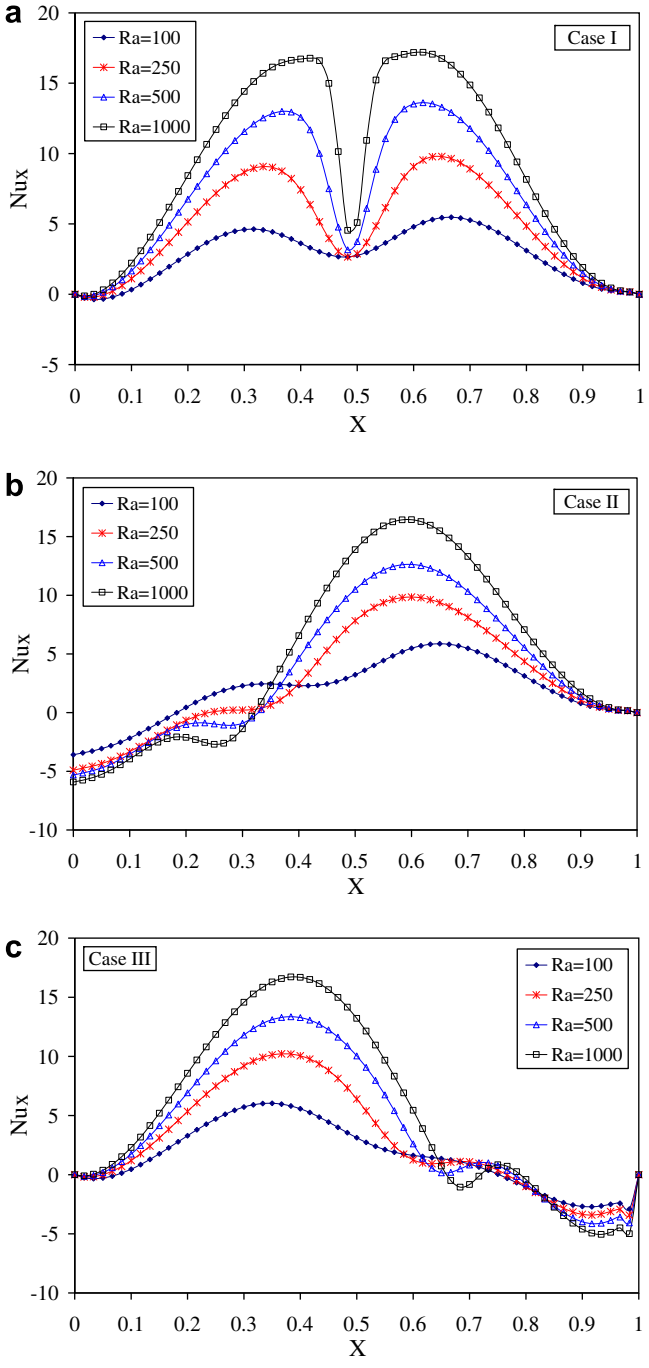


**Fig. 9.** Variation of local Nusselt number along the bottom wall for different Darcy-modified Rayleigh numbers at *AR* = 1.0, (a) Case I, (b) Case II, (c) Case III.

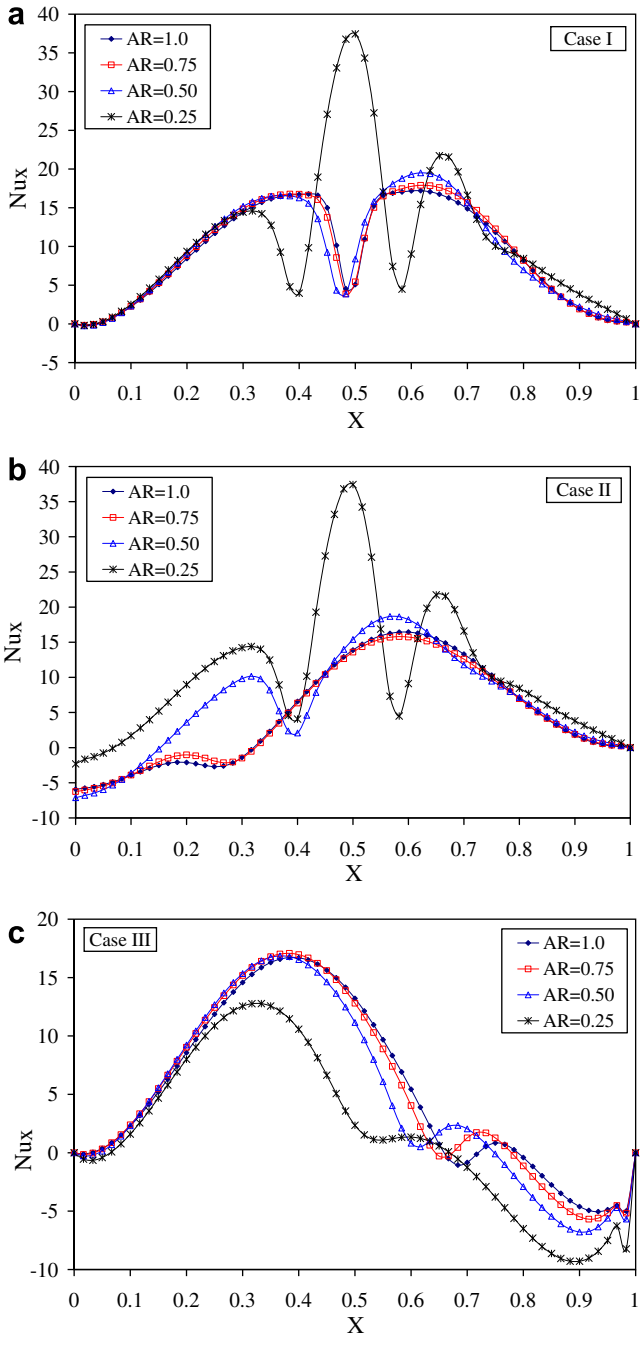


**Fig. 10.** Variation of local Nusselt number along the bottom wall for different aspect ratios at *Ra* = 1000, (a) Case I, (b) Case II, (c) Case III.

ditions. It means that the direction of heat transfer is different. Thus, mean Nusselt numbers were calculated from the positive values and presented in Figs. 11 and 12 for different Darcy-modified Rayleigh number and aspect ratio AR, respectively. Calculation was made using Eq. (19). As plotted in Fig. 11 that mean Nusselt number for Case I is higher than that of Case II and III and it is almost the same for II and III. Globally, the mean Nusselt number is an increasing function of Darcy-modified Rayleigh number on non-isothermal wall. This result has been also found in the study of Bilgen and Ben Yedder [12], which is on sinusoidally heated enclosure. Differences between Nusselt numbers increase with the increasing of Darcy-modified Rayleigh number due to increasing of domination of convection mode of heat transfer. Fig. 12 shows the variation of mean Nusselt number with aspect ratio for $Ra = 1000$. As seen from this figure there is again a higher heat transfer as that observed in the Case I. The trend of mean Nusselt number with AR is almost the same as that for Cases I and II and it decreases with increasing of aspect ratio AR. On the contrary, heat transfer increases with increasing of AR for Case III. Variation of mean Nusselt numbers becomes constant for AR > 0.50. This result is valid for all three cases considered.

### 5.2. On flow field

Finally, we compared the obtained results showing the maximum values of the stream function. These results give an idea on flow strength or measure of intensity of the flow and extent of the recirculation region. Fig. 13 shows the variation of the maximum stream function with Darcy-modified Rayleigh number for three cases considered at AR = 1.0 and the variation of the maximum stream function with the aspect ratio AR is given in Fig. 14 for $Ra = 1000$. These two figures indicate that the values of the stream function are increased with increasing both aspect ratio and Darcy-modified Rayleigh number. Lower flow strength is observed in Case I and the highest one in Case III, respectively. Obtained results for variation of stream function are supported by the study of Sarris et al. [10].

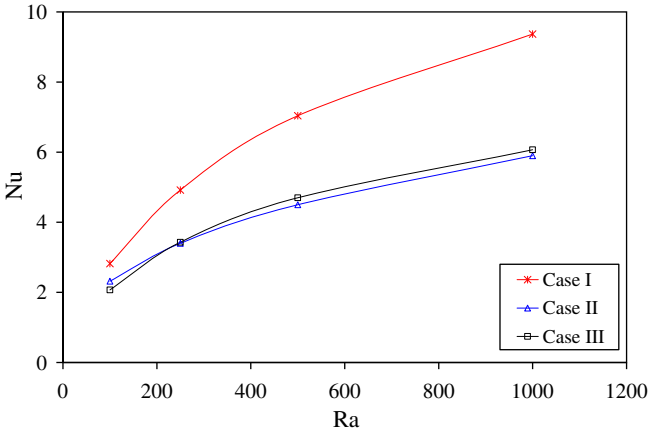


**Fig. 11.** Variation of mean Nusselt number with Darcy-modified Rayleigh number for different cases at AR = 1.0.

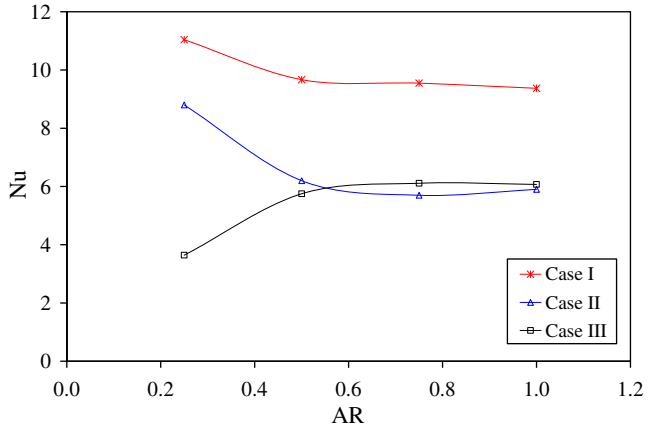


**Fig. 12.** Variation of mean Nusselt number with aspect ratio for different cases at $Ra = 1000$.

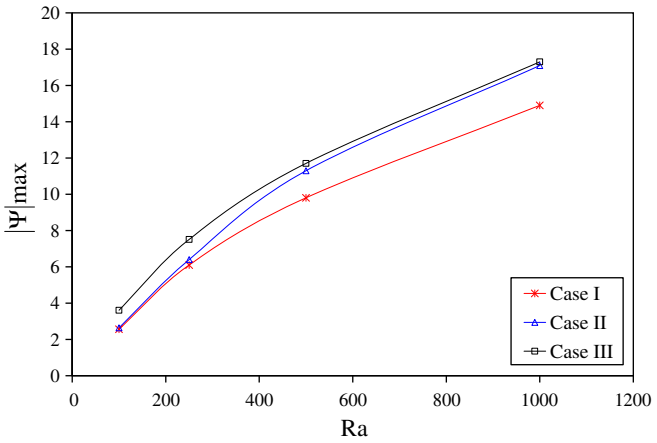


**Fig. 13.** Variation of the absolute streamfunction with Darcy-modified Rayleigh number for different cases at $AR = 1.0$.

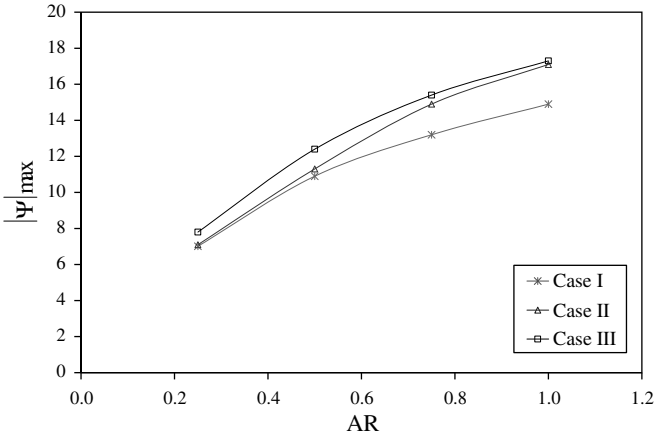


**Fig. 14.** Variation of absolute streamfunction with aspect ratio for different cases at $Ra = 1000$.

## 6. Conclusion

Three different temperature boundary conditions were tested for the problem of natural convection in a non-isothermal triangular enclosure using the heatline method. We tested the results for different Darcy-modified Rayleigh numbers $Ra$ and aspect ratios AR. Heatline method was used to visualize heat transport inside the enclosure. Important findings from the study may be drawn as follow:

(a) Heat transfer, flow field and temperature distribution are strongly affected by changing of temperature boundary conditions at vertical and inclined walls.

(b) Heatline visualization technique is a useful method that gives information on heat transport from the heated and cooled region inside the porous triangular enclosure with non-isothermal boundary conditions.
(c) Aspect ratio affects the amount of circulation mass inside the enclosure and it also affects the heat transfer depending on the boundary conditions. Heat transfer increases with aspect ratio only for Case III. For AR > 0.50, aspect ratio becomes insignificant on heat transfer.
(d) Heat transfer is an increasing function of Darcy-modified Rayleigh number for all cases. Conduction becomes dominant at small Darcy-modified Rayleigh number. Higher heat transfer is observed in Case I.
(e) Finally, application of temperature boundary conditions as Case I is better from the heat transfer point of view. To achieve this result, higher Darcy-modified Rayleigh number and lower aspect ratio are necessary.

## Acknowledgement

The authors wish to express their very sincerely thanks to the reviewers for their valuable comments and suggestions.

## References

[1] D.A. Nield, A. Bejan, Convection in Porous Media, third ed., Springer, New York, 2006.
[2] K. Vafai, Handbook of Porous Media, Marcel Dekker, New York, 2000.
[3] D.B. Ingham, I. Pop, Transport Phenomena in Porous Media, Pergamon, Oxford, 1998.
[4] A. Bejan, On the boundary layer regime in a vertical enclosure filled with a porous medium, Lett. Heat Mass Transfer 6 (1979) 93–102.
[5] B. Goyeau, J.P. Songbe, D. Gobin, Numerical study of double-diffusive natural convection in a porous cavity using the Darcy-Brinkman formulation, Int. J. Heat Mass Transfer 39 (1996) 1363–1378.
[6] R.J. Gross, M.R. Bear, C.E. Hickox, The application of flux-corrected transport (FCT) to high Rayleigh number natural convection in a porous medium, in: Proc. 8th Int. Heat Transfer Conf., San Francisco, CA, 1986.
[7] D.M. Manole, J.L. Lage, Numerical benchmark results for natural convection in a porous medium cavity, in: Heat and Mass Transfer in Porous Media ASME Conf. HTD-216, 1992, pp. 55–60.
[8] N.H. Saeid, I. Pop, Natural convection from a discrete heater in a square cavity filled with a porous medium, J. Porous Media 8 (2005) 55–63.
[9] A.C. Baytas, I. Pop, Free convection in a square porous cavity using a thermal nonequilibrium model, Int. J. Therm. Sci. 41 (2002) 861–870.
[10] I.E. Sarris, I. Lekakis, N.S. Vlachos, Natural convection in a 2D enclosure with sinusoidal upper wall temperature, Numer. Heat Transfer, Part A 42 (2002) 513–530.
[11] A. Dalal, M.K. Das, Natural convection in a cavity with a wavy wall heated from below and uniformly cooled from the top and both sides, J. Heat Transfer 128 (2006) 717–725.
[12] E. Bilgen, R. Ben Yedder, Natural convection in enclosure with heating and cooling by sinusoidal temperature profiles on one side, Int. J. Heat Mass Transfer 50 (2007) 139–150.
[13] N.H. Saeid, Natural convection in porous cavity with sinusoidal bottom wall temperature variation, Int. Commun. Heat Mass Transfer 32 (2005) 454–463.
[14] Y. Varol, H.F. Oztop, I. Pop, Numerical analysis of natural convection for a porous rectangular enclosure with sinusoidally varying temperature profile on the bottom wall, Int. Commun. Heat Mass Transfer 35 (2008) 56–64.
[15] H. Asan, L. Namli, Numerical simulation of buoyant flow in a roof of triangular cross-section under winter day boundary conditions, Energy Buildings 33 (2001) 753–757.
[16] G. Wang, An efficient equal-order finite-element method for natural convection in complex enclosures, Numer. Heat Transfer, Part B 42 (2002) 307–324.
[17] A.C. Baytas, I. Pop, Free convection in oblique enclosures filled with a porous medium, Int. J. Heat Mass Transfer 42 (1999) 1047–1057.
[18] T.S. Lee, Numerical experiments with fluid convection in tilted nonrectangular enclosures, Numer. Heat Transfer, Part A 19 (1991) 487–499.
[19] F. Moukalled, M. Darwish, Natural convection in a partitioned trapezoidal cavity heated from the side, Numer. Heat Transfer, A Appl. 43 (2003) 543–563.
[20] Y. Varol, H.F. Oztop, I. Pop, Numerical analysis of natural convection in an inclined trapezoidal enclosure filled with a porous medium, Int. J. Therm. Sci., doi:10.1016/j.ijthermalsci.2007.10.018.
[21] M. Boussaid, A. Djerrada, M. Bouhadef, Thermosolutal transfer within trapezoidal cavity, Numer. Heat Transfer, Part A 43 (2003) 431–448.
[22] S. Kimura, A. Bejan, The heatline visualization of convective heat transfer, J. Heat Transfer 105 (1983) 916–919.
[23] A.M. Morega, A. Bejan, Heatline visualization of forced convection laminar boundary layers, Int. J. Heat Mass Transfer 36 (1993) 3957–3966.
[24] S.K. Dash, Heatline visualization in turbulent flow, Int. J. Numer. Methods Heat Fluid Flow 6 (1996) 37–46.
[25] A. Dalal, M.K. Das, Heatline method for the visualization of natural convection in a complicated cavity, Int. J. Heat Mass Transfer 51 (2008) 263–272.
[26] V.A.F. Costa, Unified streamline heatline and massline methods for the visualization of two-dimensional heat and mass transfer in anisotropic media, Int. J. Heat Mass Transfer 46 (2003) 1309–1320.
[27] V.A.F. Costa, Bejan's heatlines and masslines for convection visualization and analysis, Appl. Mech. Rev. 59 (2006) 126–145.
[28] F.Y. Zhao, D. Liu, G.F. Tang, Conjugate heat transfer in square enclosures, Heat Mass Transfer 43 (2007) 907–922.
[29] M. Mobedi, Conjugate natural convection heat transfer in a square cavity with finite thickness horizontal walls, Int. Commun. Heat Mass Transfer 35 (2008) 503–513.
[30] Q.H. Deng, G.F. Tang, Numerical visualization of mass and heat transport for conjugate natural convection/ heat conduction by streamline and heatline, Int. J. Heat Mass Transfer 45 (2002) 2373–2385.
[31] A.M. Al-Amiri, Analysis of momentum and energy transfer in a lid-driven cavity filled with a porous medium, Int. J. Heat Mass Transfer 43 (2000) 3513–3527.
[32] P.M. Haese, M.D. Teubner, Heat exchange in an attic space, Int. J. Heat Mass Transfer 45 (2002) 4925–4936.